Optimizing single-photon quantum radar detection through partially postselected filtering

Liangsheng Li,[1,*] Maoxin Liu,[2] Wen-Long You,[3] Chengjie Zhang,[4] Shengli Zhang,[5] Hongcheng Yin,[1] Zhihe Xiao,[1] and Yong Zhu[1]

[1]*National Key Laboratory of Scattering and Radiation, Beijing 100854, China*
[2]*School of Systems Science and Institute of Nonequilibrium Systems, Beijing Normal University, Beijing 100875, China*
[3]*College of Physics, Nanjing University of Aeronautics and Astronautics, Nanjing 211106, China*
[4]*School of Physical Science and Technology, Ningbo University, Ningbo 315211, China*
[5]*Center for Quantum Technology Research, School of Physics, Beijing Institute of Technology, Beijing 100081, China*

(Received 12 June 2023; revised 13 October 2023; accepted 23 February 2024; published 7 March 2024)

In this study, we explore an approach aimed at enhancing the transmission or reflection coefficients of absorbing materials through the utilization of joint measurements of entangled photon states. On the one hand, through the implementation of photon catalysis in the reflected channel, we can effectively modify the state of the transmission channel, leading to a notable improvement in the transmission ratio. Similarly, this approach holds potential for significantly amplifying the reflection ratio of absorbing materials, which is useful for detecting cooperative targets. On the other hand, employing statistical counting methods based on the technique of heralding on zero photons, we evaluate the influence of our reflection enhancement protocol for detecting noncooperative targets, which is validated through Monte Carlo simulations of a quantum radar setup affected by Gaussian white noise. Our results demonstrate a remarkable enhancement in the signal-to-noise ratio of imaging, albeit with an increase in mean-square error. These findings highlight the potential practical applications of our approach in the implementation of quantum radar.

DOI: 10.1103/PhysRevA.109.033704

I. INTRODUCTION

Radar is a highly effective device that utilizes electromagnetic signals to detect and determine the range of unknown targets [1]. Over the past few decades, scientists have conducted extensive theoretical and experimental research to enhance the performance of realistic radar systems. In all radar systems, a high signal-to-noise ratio (SNR) plays a key role that determines the sensitivity and efficiency in realistic target detection. To improve the SNR, the most straightforward approach is to employ optical or microwave photon detectors that possess both high sensitivity and high detection efficiency. Ultrasensitive detectors that are capable of counting single photons or even single microwave photons have been developed, providing a substantial enhancement in accuracy compared to conventional radar systems. The quantum effects at the single-photon level are negligible, undoubtedly heralding a new era of quantum radar in which techniques from quantum information science are harnessed for precise positioning, ranging, and detection of conventional targets. Meanwhile, quantum information science has become a flourishing interdisciplinary field that combines quantum mechanics, computation, and information theory. Using quantum mechanics principles, quantum information science adopts a revolutionary approach to encode, store, transmit, and manipulate information [2,3] which seeks to successfully surpass the performance limits of classical information systems. For example, quantum metrology, in which quantum entangled states are prepared as probes and interferometric measurements are conducted during the probe readout, can potentially reach the sensitivity limit dictated by Heisenberg's principle [4–7]. This implies that the number of repetitions needed to achieve a certain level of precision is merely the square root of that required in classical measurement strategies, providing a quadratic acceleration of the measurement process.

Entanglement quantum radar was pioneered by Lloyd [8] and is alternatively referred to as quantum illumination radar, which represents a genuine quantum radar system, wherein quantum entanglement is sent to interrogate the target and joint quantum measurements are used to detect the resulting echo signal. Many sophisticated techniques, such as efficient entanglement generation, optimized discrimination of quantum states, manipulation of photon numbers using photon catalysis, and high-resolution single-photon detection in optical and microwave regimes, can be seamlessly integrated into quantum radar systems, making them increasingly suitable for various commercial and military applications. Various types of quantum states have undergone testing and evaluation in the context of entanglement quantum radar, including photon-number correlation states [9], N-entangled photons [10], two-mode squeezing states (TMSSs) [11], photon-subtracted TMSSs [12], photon-added TMSSs [13], multimode quantum entanglement states [14], x-ray quantum entanglement [15], and even microwave quantum entanglement states [16]. Typically, achieving a 6-dB advantage over conventional radar through entanglement quantum illumination necessitates the

*liliangshengbititp@163.com

implementation of joint quantum measurements on all echo signals and auxiliary entangled modes [17]. To alleviate the substantial demands on quantum storage capacity, more efficient joint-measurement-free measurement schemes become imperative. A mode-by-mode scheme for a quantum receiver with balanced homodyne measurement and optical parametric amplification was designed [18]. Zhang *et al.* proposed to use noiseless linear amplification to enhance the receiver [19], which is also applicable to quantum illumination with Gaussian states [20]. An optimal receiver utilizing iterative sum-frequency generation was proposed, demonstrating the possibility of achieving the quantum Chernoff bound for quantum illumination in the low-signal brightness limit [21].

To further explore the unprecedent potential of quantum radar, various characteristics of quantum radar have been theoretically studied. The quantum radar cross section (QRCS) was introduced via quantum electrodynamics and interferometric principles [22] and has mainly been explored theoretically. A closed-form expression for and analysis of the slumping effect of a cuboid in the scattering characteristics of quantum radar were derived [23]. Furthermore, a method for calculating the orthogonal projected area of a target in each incidence, which is a key component in determining the QRCS of any arbitrary three-dimensional convex target, was determined [24]. Entanglement quantum radar can enhance various applications, including data reading [25,26], imaging [27], velocity measurement [28], target ranging [29], and biomedical imaging [30,31]. Additionally, research has explored the enhancement of lidar through quantum entanglement [32]. More importantly, recent experiments in quantum radar made significant progress [33–35].

However, most of the results concerning entanglement quantum radar assume cooperative targets that are highly reflective and lossless. In practical scenarios, it is more likely that the target is noncooperative or even offensive, especially when covered with absorbing materials. In such cases, the reflectivity or transmissibility of the target is extremely low, posing a challenge to collecting sufficient echo signals for effective quantum measurements. Consequently, a photon-filtering strategy that can potentially improve the transmission or reflection coefficients of noncooperative targets becomes very important in all quantum radar systems. In this work, we propose a photon-filtering scheme to enhance the transmission coefficients which can be easily adapted to enhance the reflection coefficients. Moreover, we introduce two methods to implement the photon-filtering scheme. The first method is based on photon catalysis [36–41], and the second method involves the technique of heralding on zero photons [42]. Both approaches can significantly improve the imaging of absorbing targets.

The rest of this paper is organized as follows. In Sec. II, we illustrate the effective enhancement of transmission or reflection signals through the utilization of a partially postselected quantum filter. Section III introduces the implementation of the photon catalysis, which is useful for detecting cooperative targets. Based on the technique of heralding on zero photons [42], we present another photon-filtering scheme for detecting noncooperative targets in Sec. IV. We employ statistical counting methods to simulate the effects of reflection enhancement and demonstrate the effectiveness of our enhancement scheme for significantly improving the SNR of imaging through a Monte Carlo simulation on Gaussian white noise. Finally, Sec. V summarizes our results.

II. PARTIALLY POSTSELECTED FILTER

In this section, we illustrate how the transmission signal or the reflection signal is effectively enhanced. The main idea is to manipulate a quantum state to be measured by encoding a prepared parameter. To be concrete, photon filtering is employed to enhance the target signal. The photon filtering employed in this work utilizes a form of postselection [43,44]. Past research has shown that postselection can significantly alter photon statistics [45–48]. Recent theoretical research has suggested that postselected quantum experiments have the potential to surpass the Heisenberg limit by allowing quantum states to carry additional Fisher information [49]. Such benefit may be connected to the negative quasiprobability distribution [50–54]. Improved quantum advantages can be attained when properly conditioned experiments are performed with a lower rate of successful postselection [55,56]. Notably, in a recent polarimetry experiment, a quantum postselection protocol substantially elevated the precision of per-detected photons by more than 2 orders of magnitude [44]. This progress inspires us to explore the potential for improving the measurement of the SNR in reflections by devising a postselection protocol involving an absorbing material.

Consider a photon state

$$|s\rangle = \sum_n c_n |n\rangle, \tag{1}$$

where $|n\rangle$ represents a photonic Fock state. The photon-filtering-based noiseless quantum amplifiers are produced using the nonunitary operation [57]

$$G_{sc} = \frac{1}{g}(|0\rangle\langle 0| + g|1\rangle\langle 1|), \tag{2}$$

where $g > 1$ is the gain. Then applying G_{sc} acting on the state $|s\rangle$, one readily obtains the state

$$|qs\rangle = \frac{c_0}{g}|0\rangle + gc_1|1\rangle. \tag{3}$$

The components other than $|0\rangle$ and $|1\rangle$ are eliminated from the state $|qs\rangle$. For convenience, we apply the partially postselected filter, which is defined by the operator via conditional measurements:

$$F = |0\rangle\langle 0| + p|1\rangle\langle 1|, \tag{4}$$

in which p is a postselection parameter. We will see in the following that a partially postselected quantum filter can be utilized to effectively improve both the transmission and the reflection of a single-photon-state input.

Enhanced transmission based on a quantum filter. First, we discuss the scheme to enhance the transmission using the partially postselected quantum filter, as illustrated in Fig. 1(a). The setup consists of three parts, including two-channel scattering, a partially postselected quantum filter, and a signal counter module. The two-channel scattering is implemented by a beam splitter, which is a finite-thickness slab, as shown in Fig. 1(a). There are two channels of inputs, including input

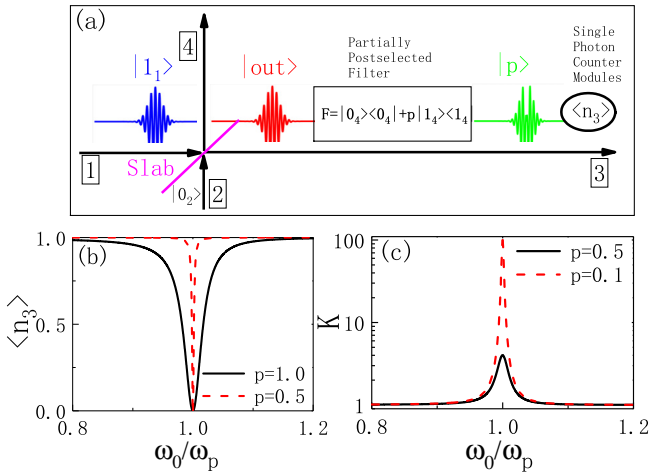

FIG. 1. (a) An implementation of a partially postselected filter via conditional measurements in a beam splitter. A single photon is prepared in the input mode of a dispersion beam splitter with reflectivity $|r(\omega)|^2$. The incident angle is $\theta = \pi/4$. The performance of the partially postselected filter with different postselection parameters is shown. (b) The average photon number in channel 3 versus incident frequency. (c) The amplification ratio versus incident frequency. Increasing p reduces the amplification.

mode 1 of a single-photon state and input mode 2 of the vacuum state, which are divided by the beam splitter into the outputs of modes 3 and 4. Assuming that in the dispersive slab the absorption might be neglected, the input-output formalism between the annihilation operators of input modes $\vec{P}^T = (a_1(\omega), a_2(\omega))^T$ and output modes $\vec{O}^T = (a_3(\omega), a_4(\omega))^T$ can then be described by a linear relation as

$$\vec{O} = \mathcal{T}(\omega) \cdot \vec{P}, \tag{5}$$

where the operators of each channel are assumed to satisfy the following commutation relations:

$$[a_\alpha(\omega), a_\beta^\dagger(\omega')] = \delta(\omega - \omega')\delta(\alpha - \beta),$$
$$[a_\alpha(\omega), a_\beta(\omega')] = [a_\alpha^\dagger(\omega), a_\beta^\dagger(\omega')] = 0. \tag{6}$$

The transformation matrix $\mathcal{T}(\omega) \in \mathrm{SU}(2)$ is a unitary matrix, i.e., $\mathcal{T}^\dagger(\omega)\mathcal{T}(\omega) = I$, and thus can be explicitly expressed as

$$\mathcal{T}(\omega) = \begin{pmatrix} t(\omega) & r(\omega) \\ -r^*(\omega) & t^*(\omega) \end{pmatrix}. \tag{7}$$

Here $r(\omega)$ and $t(\omega)$ are reflection and transmission coefficients, respectively.

In order to determine the transformation matrix $\mathcal{T}(\omega)$ of the dispersive slab, we adopt the lossless Drude model, where the permittivity is $\varepsilon = 1 - \omega_p^2/\omega^2$ and the permeability is $\mu = 1$. Without loss of generality, we choose a set of typical parameters of the beam splitter. The plasma frequency is $\omega_p = 10^{14}$ Hz, and the slab thickness is $L = 3$ μm. Thus, the reflection and transmission coefficients of the beam-splitter model with an incident angle θ are given by

$$t(\omega) = \frac{\alpha}{\beta^2 - 1} e^{-i\bar{\omega}\cos\theta}, \quad r(\omega) = \frac{\alpha\beta - \beta^2 + 1}{\beta^2 - 1}, \tag{8}$$

with the parameters

$$\bar{\omega} = \frac{\omega}{\omega_p},$$
$$\alpha = 4D\bar{\omega}\cos\theta(D^2 + \sin^2\theta)(e^{-iD} - e^{iD}),$$
$$\beta = \frac{(D^2 + \sin^2\theta)(e^{-iD} - e^{iD}) + D\bar{\omega}\cos\theta(e^{-iD} + e^{iD})}{2D\bar{\omega}\cos\theta},$$
$$D = \sqrt{(\bar{\omega}\cos\theta)^2 - 1}. \tag{9}$$

With an explicit description of the transformation matrix $T(\omega)$, we can accurately compute the scattering process of the beam splitter. To proceed, we focus on a single-photon state residing in mode 1, characterized by solely positive frequencies, which is defined as

$$|1_1\rangle = \int_0^\infty d\omega\Gamma(\omega)a_1^\dagger(\omega)|0_1\rangle, \tag{10}$$

where $\Gamma(\omega)$ is the frequency distribution function. Mode 2 is initially prepared in the vacuum state $|0_2\rangle$. Thus, the input state is

$$|\mathrm{in}\rangle = \int_0^\infty d\omega\Gamma(\omega)a_1^\dagger(\omega)|0_1\rangle \otimes |0_2\rangle, \tag{11}$$

satisfying

$$\langle\mathrm{in}|\mathrm{in}\rangle = \int_0^\infty d\omega|\Gamma(\omega)|^2 = 1. \tag{12}$$

According to the input-output formalism, the output mode can be given by

$$|\mathrm{out}\rangle = \int_0^\infty d\omega\Gamma(\omega)\big[t(\omega)a_3^\dagger(\omega) - r^*(\omega)a_4^\dagger(\omega)\big]|0\rangle. \tag{13}$$

The state $|\mathrm{out}\rangle$ is an entangled state. To clearly see it, we rewrite Eq. (13) as

$$|\mathrm{out}\rangle = \int_0^\infty d\omega\Gamma(\omega)\big[t(\omega)\big|1_3^\omega\big\rangle \otimes \big|0_4^\omega\big\rangle - r^*(\omega)\big|0_3^\omega\big\rangle \otimes \big|1_4^\omega\big\rangle\big]. \tag{14}$$

We then apply a partially postselected filter, which is given by

$$F_T = |0_4\rangle\langle 0_4| + p|1_4\rangle\langle 1_4|, \tag{15}$$

where the postselection parameter $|p| \in [0, 1]$. Here the partially postselected filter acts as a Kraus operator [57] for the single-photon-state input. The state $F_T|\mathrm{out}\rangle$ can be easily obtained by replacing r^* with pr^* in Eq. (13), namely,

$$F_T|\mathrm{out}\rangle = \int_0^\infty d\omega\Gamma(\omega)\big[t(\omega)a_3^\dagger(\omega) - pr^*(\omega)a_4^\dagger(\omega)\big]|0\rangle. \tag{16}$$

If we can perform a quantum state filtering on the field in mode 4, then the filter allows the $|\mathrm{out}\rangle$ state to pass with probability

$$A = \langle\mathrm{out}|F_T^\dagger F_T|\mathrm{out}\rangle. \tag{17}$$

We now focus on the photon number in the partially postselected quantum detection experiments. The postselection is realized by a projective measurement after a unitary evolution

set by the beam splitter but before the final photon detection. Then, the postselected state becomes

$$|p\rangle = F_T|\text{out}\rangle/\sqrt{A}. \tag{18}$$

Note that this state should be renormalized by the passing probability, which stems from the projective measurement implemented by the partially postselected filter with limited efficiency.

However, the filter effectively amplifies the average photon numbers in mode 3,

$$\langle n_3\rangle_p = \frac{\int_0^\infty d\omega|\Gamma(\omega)t(\omega)|^2}{\int_0^\infty d\omega|\Gamma(\omega)|^2[|t(\omega)|^2+|pr(\omega)|^2]}. \tag{19}$$

To illustrate the amplification effect occurring specifically at frequency ω_0, we employ the Dirac δ distribution, i.e.,

$$|\Gamma(\omega)|^2 = \delta(\omega-\omega_0). \tag{20}$$

In this case, the mean photon number in channel 3 can be readily obtained as

$$\langle n_3\rangle_p = \frac{T(\omega_0)}{T(\omega_0)+|p|^2R(\omega_0)}. \tag{21}$$

We observe that the $|\text{out}\rangle$ state is recovered for $p=1$ with $\langle n_3\rangle_{p=1} = T(\omega_0) < 1$, which is equal to the transmission ratio without the operation of the partially postselected filter. Another limit is the case of $p=0$ with $\langle n_3\rangle_{p=0}=1$, which implies that the effective transmission is enhanced. For a generic value of $0<p<1$, we can find from Eq. (21) that $\langle n_3\rangle_p$ is larger than $\langle n_3\rangle_{p=1}$ since positive-valued $T(\omega_0)$ and $R(\omega_0)$ satisfy the constraint that $T(\omega_0)+R(\omega_0)=1$. This clearly suggests that the partially postselected filter amplifies the average photon numbers in channel 3. To better quantify the effect, we thus define an amplified ratio given by

$$K = \frac{\langle n_3\rangle_p}{\langle n_3\rangle_{p=1}}. \tag{22}$$

The larger the ratio K is, the better the amplification effect is. A large average photon number is typically easier to detect than a smaller one. If the average photon number $\langle n_3\rangle_{p=1} \ll 1$, then the partially postselected filter boosts the amplified ratio $K \approx \frac{1}{|p|^2}$. The amplified ratio can be tuned to be arbitrarily large if $\langle n_3\rangle_{p=1}$ is arbitrarily small.

The transmission enhancement scheme is applicable not only to the δ distribution in Eq. (20) but also to the general frequency distribution of the incident state. To illustrate this, we consider a Gaussian frequency distribution:

$$\Gamma(\omega) = \frac{1}{\sqrt{\sigma\pi}} e^{-i\frac{\omega-\omega_0}{\omega_0\tau}} e^{-\frac{1}{2\sigma^2}\left(\frac{\omega-\omega_0}{\omega_0}\right)^2}. \tag{23}$$

Figure 2(a) illustrates how the average transmitted photon number $\langle n_3\rangle$ is affected by varying the value of p while keeping the width of the photon field frequency distribution fixed. As the value of p decreases, the efficiency of the transmission is improved. This effect is more prominently demonstrated in Fig. 2(b), where the gain K increases significantly with decreasing values of p. Figures 2(c) and 2(d) depict the impact of the width of the frequency distribution of the photon field on the amplification of transmission in the amplification scheme.

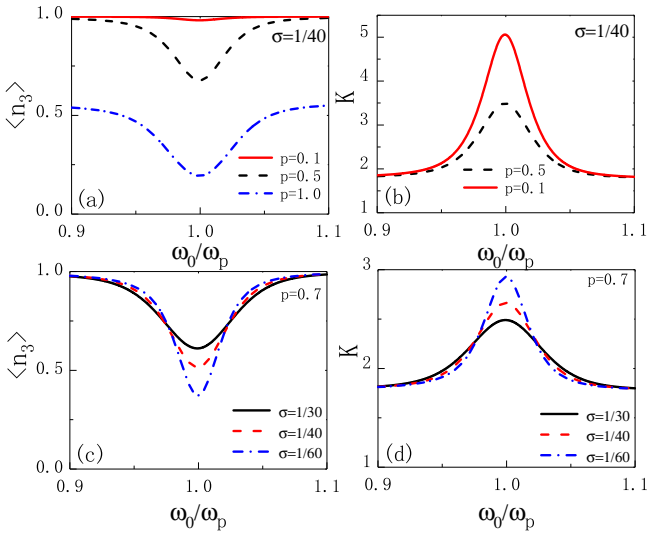

FIG. 2. The results for Gaussian frequency distribution in Eq. (23). (a) The average photon number in channel 3 $\langle n_3\rangle$ and (b) the amplification ratio K as a function of incident frequency with $\sigma = 1/40$ and $p = 0.1,\ 0.5,\ 1.0$. (c) The average photon number in channel 3 $\langle n_3\rangle$ and (d) the amplification ratio K as a function of incident frequency with $\sigma = 1/30,\ 1/40,\ 1/60$ and $p = 0.7$.

It is noteworthy that a narrower frequency distribution enhances the amplification effect, particularly in the vicinity of the center of the distribution denoted as ω_0.

III. IMPLEMENTATION OF PHOTON FILTERING BY PHOTON CATALYSIS

Section II introduced a general approach for enhancing transmission or reflection channels via photon filtering. However, the specific implementations of the photon-filtering operation in Eq. (15) have not been discussed yet. To address this gap, we will present two methods for implementing Eq. (15). The first method, based on photon-catalysis technology, is primarily utilized for cooperative targets. Figure 3 shows implementations of the photon catalysis, which effectively implements the filter in Eqs. (4) and (15). In Fig. 3(a), the transmission ratio of beam splitter BS_1 is T, and that of BS_2 is p^2. The input in channel 1 is a single-photon state, while channels 2 and 5 are in a vacuum state. If the single-photon detector obtains zero photons, the entangled state of channels 3 and 6 becomes

$$|\psi\rangle = \frac{\sqrt{T}|1\rangle|0\rangle + p\sqrt{1-T}|0\rangle|1\rangle}{\sqrt{T+(1-T)p^2}}, \tag{24}$$

from which we obtain the measured photon number in channel 3 as follows:

$$\langle n\rangle_p = \frac{T}{T+p^2(1-T)}, \tag{25}$$

which recovers Eq. (21).

However, the scheme in Fig. 3(a) requires a single-photon detector with 100% accuracy, or the single-photon state $|1\rangle$ will be faultily considered a vacuum $|0\rangle$. To accurately detect the zero-photon state at detector D_1, as shown in

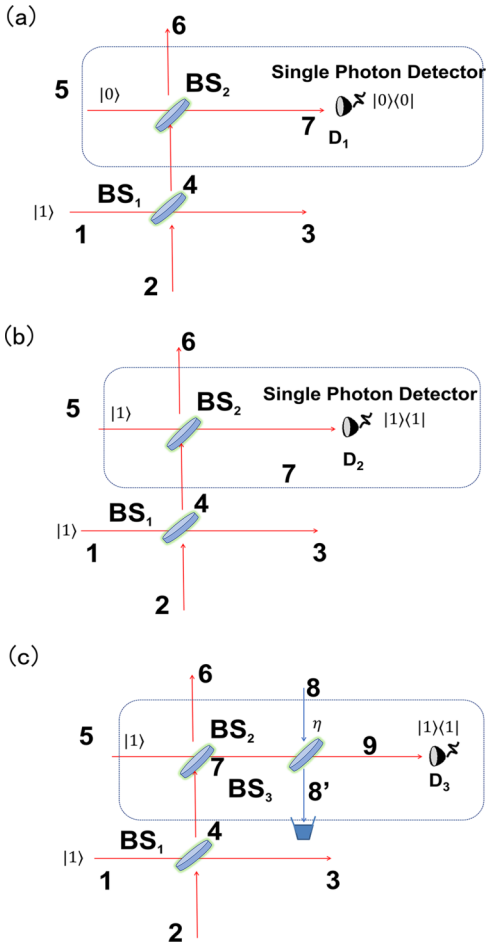

FIG. 3. A sketch for implementing quantum catalysis using (a) zero-photon detection, (b) ideal single-photon detection, and (c) realistic single-photon detection. Both detectors D_1 and D_2 are ideal single-photon detectors. The beam splitter BS_3 with a transmittance of η, combined with the ideal single-photon detector D_3 capable of photon number resolution, is used to simulate a realistic single-photon detector with detection efficiency of η. The input optical quantum states in modes 2 and 8 are the vacuum state $|0\rangle$.

Fig. 3(a), a heralding technique on detection of zero photons is necessary [42]. This, however, requires the addition of a pulsed-laser light source, increasing the complexity and cost of the setup. In this study, we propose alternative methodologies that circumvent the need for detecting the zero-photon state. Specifically, we design the alternative scheme shown in Fig. 3(b). If the single-photon detector D_2 obtains a single photon (D_2 is a photon-number-resolving detector, which can distinguish one from two photons), the entangled state of channels 3 and 6 becomes

$$|\psi\rangle = \frac{p\sqrt{T}|1\rangle|0\rangle + (2p^2-1)\sqrt{1-T}|0\rangle|1\rangle}{\sqrt{p^2T+(1-T)(2p^2-1)^2}}, \tag{26}$$

from which we obtain the measured photon number in channel 3 as follows:

$$\langle n\rangle_p = \frac{Tp^2}{p^2T+(1-T)(2p^2-1)^2}, \tag{27}$$

which also enhances the photon number.

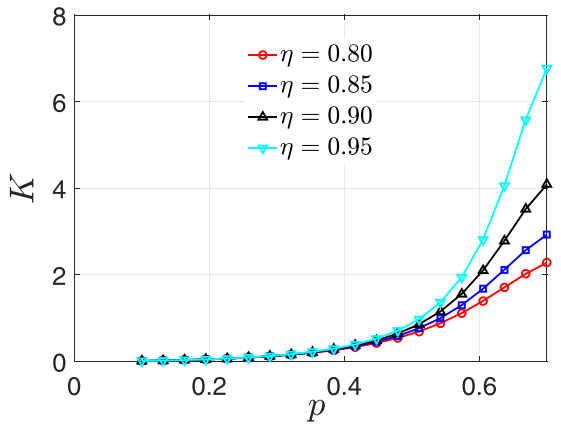

FIG. 4. Amplification ratio K as a function of p. η is chosen to be 0.80, 0.85, 0.90, and 0.95, from bottom to top.

The scheme in Fig. 3(b) also works when the detector is a realistic single-photon detector with nonunit detection efficiency. In Fig. 3(c) we use beam splitter BS_3 with transmissivity η and an ideal single-photon detector to represent a detector with efficiency η. The input modes of channels 2 and 8 are injected with the vacuum state $|0\rangle$, and the outgoing mode channel $8'$ is discarded. When detector D_3 registers a single photon, the photon catalysis process is considered successful. The probability of photon catalysis is as follows:

$$P_{\mathrm{p},\eta} = \eta[p^2T + (1-T)(4p^4\eta - 4p^2\eta + 1)], \tag{28}$$

and the output states in channels 3 and 6 are now a mixed state given by

$$\rho_{p,\eta} = \frac{4p^2(1-p^2)(1-T)\eta(1-\eta)|0\rangle|0\rangle\langle 0|\langle 0| + |\widetilde{\psi}\rangle\langle\widetilde{\psi}|}{P_{\mathrm{p},\eta}}, \tag{29}$$

with $|\widetilde{\psi}\rangle$ being an un-normalized state,

$$|\widetilde{\psi}\rangle = \sqrt{\eta}[p\sqrt{T}|1\rangle|0\rangle + \sqrt{1-T}(2p^2-1)|0\rangle|1\rangle]. \tag{30}$$

For $\eta \to 1$, it can be easily checked that $|\widetilde{\psi}\rangle$ (if normalized) is exactly the state in Eq. (26). Moreover, one can see that the nonunit detection efficiency induces a non-negligible vacuum state component $|0\rangle|0\rangle$ in $\rho_{p,\eta}$, which does not ultimately contribute to the average photon number in channel 3. This explains why the scheme shown in Fig. 3(b) remains robust even with a realistic single-photon detector. The average photon number in Fig. 3(c) is now calculated as follows:

$$\langle n\rangle_{p,\eta} = \frac{Tp^2}{p^2T+(1-T)(4p^4\eta-4p^2\eta+1)}. \tag{31}$$

The amplification ratio in the case of the nonunit detector is given by

$$K_{p,\eta} = \frac{p^2}{p^2T+(1-T)(4p^4\eta-4p^2\eta+1)}. \tag{32}$$

A large amplification ratio, $K \gg 1$, can be observed even when using realistic detectors. In Fig. 4, we show the amplification ratio for η values of 0.80, 0.85, 0.90, and 0.95. For $p > 0.5$, a rapid increase in K is observed.

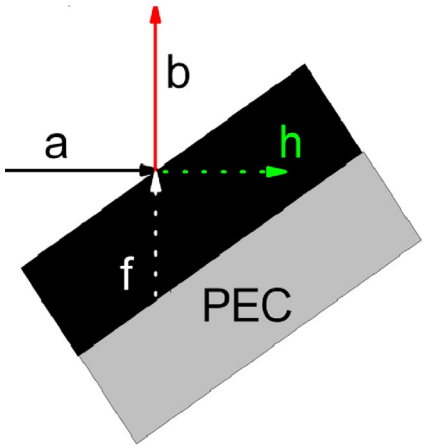

FIG. 5. A general schematic representation of a reflection system. "PEC" refers to a perfect electric conductor with total reflection, and the black portion represents its absorbing material surface. The input channel is labeled a, the reflection is denoted b, the noise from the absorbing surface is represented as f, and the transmission channel is labeled h.

Quantum radar aiming to detect the absorption. In an analogous way, the above scheme to enhance the transmission can be applied to improve the detection of the reflected signal and thus can be employed to build a quantum radar for detecting cooperative targets. Figure 5 depicts a reflection process on an absorbing material. The incidents received through channel a are split into a reflected channel and an absorbed channel on the surface, known as channel b and channel h. A noise caused by the material of channel f should be included. Comparing the transmission process in Fig. 1, there is a simple mapping relation between the indices of channels $\{1, 2, 3, 4\}$ and $\{a, f, h, b\}$.

The general relation between the input and output operators including loss is

$$\begin{pmatrix} b(\omega) \\ h(\omega) \end{pmatrix} = \mathcal{T}(\omega) \cdot \begin{pmatrix} a(\omega) \\ f(\omega) \end{pmatrix}, \tag{33}$$

where

$$\mathcal{T}(\omega) = \begin{pmatrix} r(\omega) & k(\omega) \\ -k^*(\omega) & r^*(\omega) \end{pmatrix}, \tag{34}$$

with

$$|r(\omega)|^2 + |k(\omega)|^2 = 1. \tag{35}$$

Thus, the input operators and output operators obey the commutation relations, i.e., $[\eta(\omega_1), \eta^\dagger(\omega_2)] = \delta(\omega_1 - \omega_2)$, $\eta = a, b, h, f$, while they commute otherwise. The input multimode single-photon state at channel a can be expressed as

$$|\text{in}\rangle = \int_0^\infty d\omega \Gamma(\omega) a^\dagger(\omega) \mid 0\rangle. \tag{36}$$

The scattered output field should be

$$|\text{out}\rangle = \int_0^\infty d\omega \Gamma(\omega) \big[r(\omega) b^\dagger(\omega) - k^*(\omega) h^\dagger(\omega)\big] |0\rangle. \tag{37}$$

Consider a frequency-independent quantum filter

$$F_R = |0_h\rangle\langle 0_h| + p\big|1_h^\omega\big\rangle\big\langle 1_h^\omega\big|. \tag{38}$$

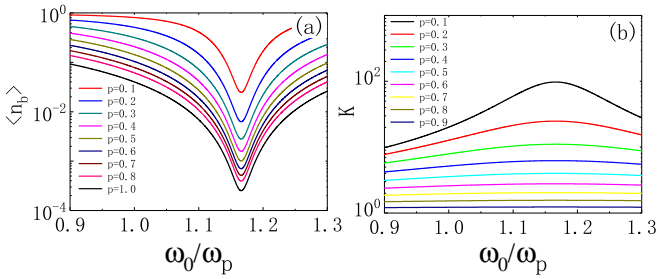

FIG. 6. (a) The average photon number in channel b and (b) the corresponding amplification ratio K as a function of incident frequency with different values of p under δ distribution.

Under the partially postselected filter, the average photon number of a multimode single-photon scattering state in channel b is

$$\langle n_b \rangle = \frac{\int_0^\infty d\omega |\Gamma(\omega) r(\omega)|^2}{|p|^2 + (1 - |p|^2) \int_0^\infty d\omega |\Gamma(\omega) r(\omega)|^2}, \tag{39}$$

and the amplified ratio is

$$K = \frac{1}{|p|^2 + (1 - |p|^2) \int_0^\infty d\omega |\Gamma(\omega) r(\omega)|^2}. \tag{40}$$

Figure 6 displays the relation between the parameter p and the average photon number in channel b under the δ distribution. In particular, Fig. 6(a) highlights that as the value of p decreases, the average photon number $\langle n_b \rangle$ gradually increases, confirming the effectiveness of our scheme in enhancing reflection. Furthermore, Fig. 6(b) presents a visually striking representation, illustrating that the enhancement effect becomes more pronounced as p increases.

IV. IMPLEMENTATION OF PHOTON FILTERING BY HERALDING ON ZERO PHOTONS

A crucial ingredient in the transmission-enhancement and reflection-enhancement schemes described above is the realization of the photon-filtering scheme, which implements operators F_T and F_R, respectively. To implement the photon-filtering scheme as outlined in Eq. (15), we propose a second method for detecting noncooperative targets. This method utilizes a heralding technique on zero photons [42] to achieve signal enhancement.

Figure 7 shows the scheme we designed. The basic physical process of this device is as follows. A photon with a frequency of 2ω is generated by the ultrapulse laser, and is subsequently converted into a pair of entangled photons, both with a frequency of ω, through a parametric down-conversion process using the β-barium borate crystal (BBO). One entangled photon enters the reflection system, and one enters the auxiliary optical path. In the reflection system, the reflection and transmission of photons are determined by the reflection matrix. In other words, this photon has a probability of $|r|^2$ of being captured by detector D_3. In the auxiliary light path, another photon is reflected with a probability of p^2, and the probability of detection by detector D_2 is also p^2.

In order to achieve signal enhancement, it is necessary to repeat the above process many times. Through this

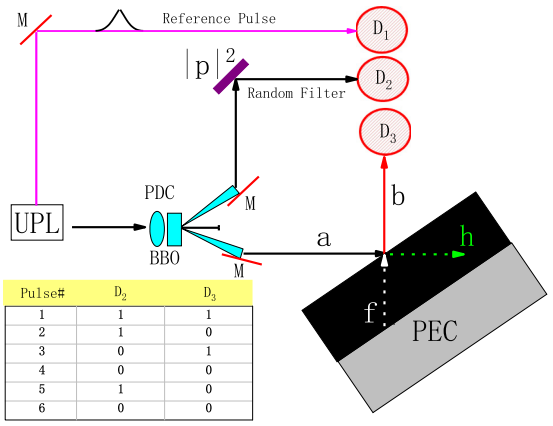

FIG. 7. An implementation of the partially postselected filter using the technique of heralding on zero photons. The lower left corner of the illustration shows a list of correlated measurement data.

iterative procedure, we obtain a data list, as depicted in the bottom left corner of Fig. 7. Suppose the number of entangled photon pairs produced by BBO is N. Detectors D_2 and D_3 are measured at the same time. $N(D_2, D_3)$ denotes the times of coincidence counting when D_2 and D_3 simultaneously obtain readings. $N(D_2, 0)$ indicates the number of times D_2 has a reading but D_3 has no reading. $N(0, D_3)$ indicates the number of times D_3 has a reading but D_2 has no reading. $N(0, 0)$ indicates the number of times D_2 and D_3 have no readings at the same time. It is worth noting that $N(D_2, 0)$, $N(0, D_3)$, and $N(0, 0)$ can be measured using the technique of heralding on zero photons [42]. Based on the principle of probability, we can establish a relationship between $\{N,\ N(D_2, D_3),\ N(D_2, 0),\ N(0, D_3),\ N(0, 0)\}$ and $\{r,\ p\}$. These entities are interconnected in the following manner:

$$\begin{aligned} N(D_2, D_3)/N &= R|p|^2, \\ N(D_2, 0)/N &= (1-R)|p|^2, \\ N(0, D_3)/N &= R(1-|p|^2), \\ N(0, 0)/N &= (1-R)(1-|p|^2). \end{aligned} \tag{41}$$

Accordingly, we can construct a measured quantity, given by

$$M(T, p) \equiv \frac{N(1,1)+N(0,1)}{N-N(0,0)} = \frac{|r(\omega)|^2}{|p|^2+(1-|p|^2)|r(\omega)|^2}. \tag{42}$$

Considering the relation

$$\langle n_b \rangle = \frac{|r(\omega)|^2}{|p|^2+(1-|p|^2)|r(\omega)|^2}, \tag{43}$$

we can readily find

$$M(T, p) = \langle n_b \rangle. \tag{44}$$

This means that the measurement of $\langle n_b \rangle$ can be replaced by the statistical measurement of M.

In practical experiments, the value of $M(T, p)$ not only is determined by Eq. (42) but also includes fluctuations. Specifically, after considering the fluctuation effect, $M(T, p)$ can be

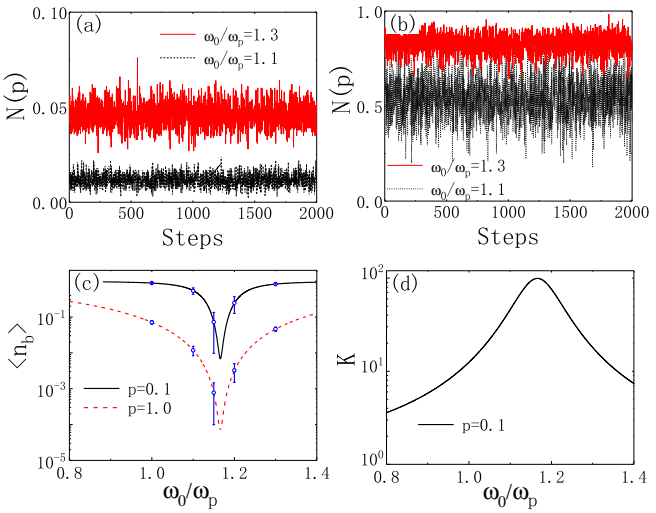

FIG. 8. Illustration of the details of the Monte Carlo simulation. (a) and (b) show the simulation values of N $[M(T, p)]$ spanning 2000 Monte Carlo steps at different frequencies ω_0/ω_p for two different values of p. Here $p = 1$ for (a), and $p = 0.1$ for (b). (c) The average effective reflection photon number as a function of frequency ω_0/ω_p for different values of parameter p (1 and 0.1). (d) The gain K as a function of frequency ω_0/ω_p for a specific value of $p = 0.1$.

represented as

$$M(T, p) = \frac{N(1,1)+\Delta N(1,1)+N(0,1)+\Delta N(0,1)}{N-[N(0,0)+\Delta N(0,0)]}. \tag{45}$$

Without loss of generality, $M(T, p)$ can be further simplified into

$$M(T, p) = \frac{N(1,1)+N(0,1)}{N-N(0,0)} + \Delta. \tag{46}$$

The Δ term in Eq. (46) encompasses all fluctuation effects and is assumed to follow a Gaussian noise distribution, characterized by the probability density function as

$$f(\Delta) = \frac{1}{\sqrt{2\pi}\sigma} \exp\left(-\frac{\Delta^2}{2\sigma^2}\right). \tag{47}$$

The Monte Carlo (MC) simulation results for the $M(T, p)$ behavior are shown in Fig. 8. The following outlines the steps of the MC simulation. First, given a frequency ω_0/ω_p and a specific value of p, we generate a data list as depicted in Fig. 7 under these conditions. In each row, the value of D_2 is 1 with probability p^2 and 0 with probability $1-p^2$, and the value of D_3 is 1 with probability $|r|^2$ and 0 with probability $1-|r|^2$. In our simulation process, the list length is 1000. Then, from the data list we can count four values of $N(D_2, D_3)$. In addition, we also need to consider the noise term in the formula in Eq. (46), which is also calculated by random-number simulation. Gathering all these, we can obtain the value of $M(T, p)$. In order to account for the average impact of various noise sources, we evaluate 2000 different noise samples for a given frequency ω_0/ω_p and a postselection parameter p. The simulation results for several specific frequencies ω_0/ω_p and p parameters are shown in Figs. 8(a) and 8(b). By averaging these simulation results, we can obtain

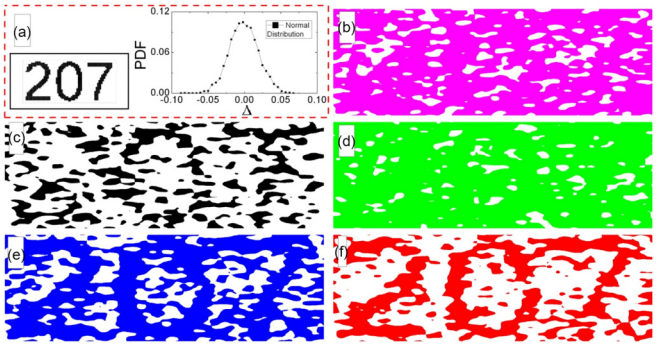

FIG. 9. Illustration of the imaging simulation. (a) The material with the pattern of the number 207, where the white part has the property of complete reflection and the black part is made of absorbing material. The inset in (a) shows a normal noise distribution with the standard deviation $\sigma = 0.02$. (b) to (f) depict the imaging results as the parameter p gradually decreases, with $p = 1.0, 0.8, 0.6, 0.4, 0.2$, respectively.

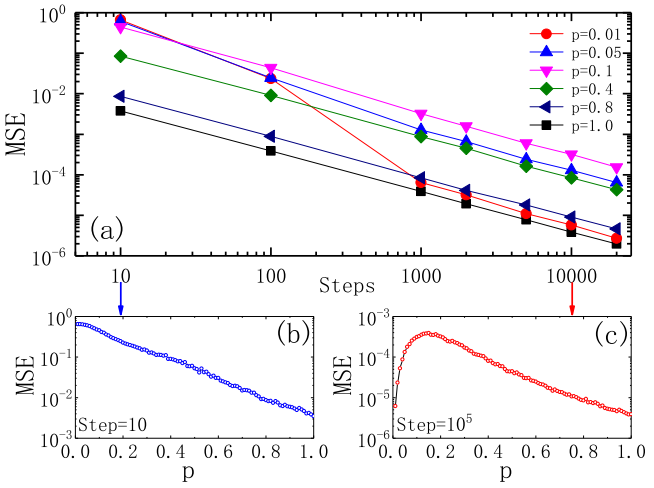

FIG. 10. (a) The MSE versus the number of independent measurements for different values of the postselection parameter p with $r = 0.2$. The MSE is calculated by repeating $N = 1000$ photons in each measurement. The MSE with respect to p after performing a total of (b) $\mathcal{N}_{\text{step}} = 10$ and (c) $\mathcal{N}_{\text{step}} = 10^4$ independent measurements.

the relationship between the effective average reflected photon number $\langle n_b \rangle$ and frequency ω_0/ω_p. Figure 8(c) shows that for different p values, $\langle n_b \rangle$ is a function of frequency ω_0/ω_p. It can be observed that when $p = 0.1$, it effectively enhances $\langle n_b \rangle$ compared to $p = 1$ (no optimization case) throughout the frequency domain. This enhancement effect is particularly significant near the resonance frequency. Figure 8(d) depicts the change in amplification rate with respect to the frequency.

Figure 9 shows the imaging results of the medium material labeled with the number 207. We depict imaging results as the parameter p gradually decreases, with $p = 1, 0.8, 0.6, 0.4, 0.2$. In Fig. 9(b), the original imaging result is shown with $p = 1$, representing no enhancement effect. Due to noise, the image of the medium material is nearly indiscernible in this case. However, as the value of p decreases, the enhancement effect gradually intensifies. Consequently, in Figs. 9(c) to 9(f), the number 207 becomes progressively clearer. This visual demonstration serves as a clear and intuitive depiction of the substantial improvement in imaging enhancement achieved in this work.

Note that the photon-filtering operation defined in Eq. (2) can be implemented using the setup illustrated in Fig. 7. Consequently, the application of the partial postselection method is justified. Furthermore, it is essential to address the impact of data loss following the implementation of our scheme. Typically, the effectiveness of an estimation procedure is evaluated using the mean-square error (MSE) [49], given by

$$\text{MSE}(p) = \frac{1}{\mathcal{N}_{\text{step}}} \sum_i [M_i(T, p) - \langle n_b \rangle_i)]^2, \tag{48}$$

in which $\mathcal{N}_{\text{step}}$ represents the number of independent measurements. Figure 10 shows the MSE for different step sizes with various values of p. In Fig. 10(a), it becomes evident that the MSE for all $p < 1$ (when employing the enhanced scheme) exceeds that for $p = 1$ (without utilizing the enhanced scheme). One observes that in Fig. 10(b) the MSE exhibits a downward trend as p increases. Intriguingly, at a step value of $\mathcal{N}_{\text{step}} = 10^4$, we observe that although the MSE initially rises with decreasing p, it begins to decrease after surpassing a certain threshold, approximately around $p = 0.15$. Thus, it is important to find a delicate balance between the improvement of the imaging SNR and an acceptable value of MSE for future practical applications, which has been successfully demonstrated in optical experiments, such as partially postselected amplification [44].

V. CONCLUSION

In this work, we proposed a scheme that enhances the transmission and reflection of absorbing materials. We achieved this by applying joint measurement to a pair of entangled photons, with one used as a signal and the other used as an auxiliary to enhance the signal. We first illustrated how our scheme can enhance the transmission of the incident photon state. The surface of the material acts as a beam splitter, dividing the incident photon state into the reflected and transmitted channels. Since the superposition state of these channels is entangled, we can use photon catalysis on the reflected channel to change the transmission channel state. By encoding the parameter p into the transmissive state, we showed that the transmission is effectively enhanced. Similarly, we can apply the scenario to enhance the reflection of absorbing materials. The signal channel, vacuum channel, reflection channel, and transmission channel in the transmission enhancement scheme correspond, respectively, to the signal channel, noise channel, absorption channel, and reflection channel in the reflection enhancement scheme. We apply the photon catalysis to the absorption channels, and the parameter p is encoded into the changed reflected state to enhance the reflected measurement. This results in an overall enhancement effect.

In order to experimentally implement reflection enhancement according to our scheme, we devised an approach based on heralding on zero photons that applies statistical

counting methods to simulate the effects of this enhancement. Specifically, we executed a Monte Carlo simulation on Gaussian white noise to validate our idea. The numerical tests showed that our enhancement scheme is effective for significantly improving the imaging signal-to-noise ratio. The potential implications of our research are exciting, as our approach could have practical applications in quantum radar implementation.

ACKNOWLEDGMENTS

This work is supported by the Ministry of Science and Technology of China (Grant No. 2016YFA0301300), the National Science Foundation of China (Grants No. 11604009, No. 11474211, and No. 12174194). We also acknowledge the computational support from the Beijing Computational Science Research Center (CSRC).

[1] R. V. Pound, From radar to nuclear magnetic resonance, Rev. Mod. Phys. **71**, S54 (1999).

[2] M. A. Nielsen and I. L. Chuang, *Quantum Computation and Quantum Information*, 10th anniversary ed. (Cambridge University Press, Cambridge, 2010).

[3] R. Horodecki, P. Horodecki, M. Horodecki, and K. Horodecki, Quantum entanglement, Rev. Mod. Phys. **81**, 865 (2009).

[4] V. Giovannetti, S. Lloyd, and L. Maccone, Quantum-enhanced measurements: Beating the standard quantum limit, Science **306**, 1330 (2004).

[5] V. Giovannetti, S. Lloyd, and L. Maccone, Advances in quantum metrology, Nat. Photon. **5**, 222 (2011).

[6] V. Giovannetti, S. Lloyd, and L. Maccone, Quantum metrology, Phys. Rev. Lett. **96**, 010401 (2006).

[7] S. L. Braunstein and C. M. Caves, Statistical distance and the geometry of quantum states, Phys. Rev. Lett. **72**, 3439 (1994).

[8] S. Lloyd, Enhanced sensitivity of photodetection via quantum illumination, Science **321**, 1463 (2008).

[9] A. Meda, E. Losero, N. Samantaray, F. Scafirimuto, S. Pradyumna, A. Avella, I. Ruo-Berchera, and M. Genovese, Photon-number correlation for quantum enhanced imaging and sensing, J. Opt. **19**, 094002 (2017).

[10] J. F. Smith III, Quantum entangled radar theory and a correction method for the effects of the atmosphere on entanglement, Proc. SPIE **7342**, 73420A (2009).

[11] D. Luong, C. W. S. Chang, A. M. Vadiraj, A. Damini, C. M. Wilson, and B. Balaji, Receiver operating characteristics for a prototype quantum two-mode squeezing radar, IEEE Trans. Aerosp. Electron. Syst. **56**, 2041 (2020).

[12] S. L. Zhang, J. S. Guo, W. S. Bao, J. H. Shi, C. H. Jin, X. B. Zou, and G. C. Guo, Quantum illumination with photon-subtracted continuous-variable entanglement, Phys. Rev. A **89**, 062309 (2014).

[13] L. Fan and M. S. Zubairy, Quantum illumination using non-Gaussian states generated by photon subtraction and photon addition, Phys. Rev. A **98**, 012319 (2018).

[14] E. Jung and D. Park, Quantum illumination with three-mode Gaussian state, Quantum Inf. Process. **21**, 71 (2022).

[15] E. Strizhevsky, D. Borodin, A. Schori, S. Francoual, R. Röhlsberger, and S. Shwartz, Efficient interaction of heralded X-ray photons with a beam splitter, Phys. Rev. Lett. **127**, 013603 (2021).

[16] S. Barzanjeh, S. Pirandola, D. Vitali, and J. M. Fink, Microwave quantum illumination using a digital receiver, Sci. Adv. **6**, eabb0451 (2020).

[17] S.-H. Tan, B. I. Erkmen, V. Giovannetti, S. Guha, S. Lloyd, L. Maccone, S. Pirandola, and J. H. Shapiro, Quantum illumination with Gaussian states, Phys. Rev. Lett. **101**, 253601 (2008).

[18] S. Guha and B. I. Erkmen, Gaussian-state quantum-illumination receivers for target detection, Phys. Rev. A **80**, 052310 (2009).

[19] S.-L. Zhang, K. Wang, J.-S. Guo, and J.-H. Shi, Quantum illumination with noiseless linear amplifier, Chin. Phys. Lett. **32**, 090301 (2015).

[20] A. Karsa, M. Ghalaii, and S. Pirandola, Noiseless linear amplification in quantum target detection using Gaussian states, Quantum Sci. Technol. **7**, 035026 (2022).

[21] Q. Zhuang, Z. Zhang, and J. H. Shapiro, Optimum mixed-state discrimination for noisy entanglement-enhanced sensing, Phys. Rev. Lett. **118**, 040801 (2017).

[22] M. Lanzagorta, Quantum radar cross sections, Proc. SPIE **7727**, 77270K (2010).

[23] Z. Tian, D. Wu, and T. Hu, Closed-form expressions and analysis for the slumping effect of a cuboid in the scattering characteristics of quantum radar, Opt. Express **29**, 34077 (2021).

[24] C. Fang, The simulation and analysis of quantum radar cross section for three-dimensional convex targets, IEEE Photonics J. **10**, 1 (2018).

[25] S. Pirandola, Quantum reading of a classical digital memory, Phys. Rev. Lett. **106**, 090504 (2011).

[26] G. Ortolano, E. Losero, S. Pirandola, M. Genovese, and I. Ruo-Berchera, Experimental quantum reading with photon counting, Sci. Adv. **7**, eabc7796 (2021).

[27] T. Gregory, P.-A. Moreau, E. Toninelli, and M. J. Padgett, Imaging through noise with quantum illumination, Sci. Adv. **6**, eaay2652 (2020).

[28] Q. Zhuang, Z. Zhang, and J. H. Shapiro, Entanglement-enhanced lidars for simultaneous range and velocity measurements, Phys. Rev. A **96**, 040304(R) (2017).

[29] Q. Zhuang and J. H. Shapiro, Ultimate accuracy limit of quantum pulse-compression ranging, Phys. Rev. Lett. **128**, 010501 (2022).

[30] A. M. Zheltikov and M. O. Scully, Photon entanglement for life-science imaging: rethinking the limits of the possible, Phys. Usp. **63**, 698 (2020).

[31] N. Aslam, H. Zhou, E. K. Urbach, M. J. Turner, R. L. Walsworth, M. D. Lukin, and H. Park, Quantum sensors for biomedical applications, Nat. Rev. Phys. **5**, 157 (2023).

[32] M. Lanzagorta, Amplification of radar and lidar signatures using quantum sensors, Proc. SPIE **8734**, 87340C(2013).

[33] S. Barzanjeh, S. Guha, C. Weedbrook, D. Vitali, J. H. Shapiro, and S. Pirandola, Microwave quantum illumination, Phys. Rev. Lett. **114**, 080503 (2015).

[34] C. W. S. Chang, A. M. Vadiraj, J. Bourassa, B. Balaji, and C. M. Wilson, Quantum-enhanced noise radar, Appl. Phys. Lett. **114**, 112601 (2019).

[35] E. P. Menzel, R. Di Candia, F. Deppe, P. Eder, L. Zhong, M. Ihmig, M. Haeberlein, A. Baust, E. Hoffmann, D. Ballester, K. Inomata, T. Yamamoto, Y. Nakamura, E. Solano, A. Marx, and R. Gross, Path entanglement of continuous-variable quantum microwaves, Phys. Rev. Lett. **109**, 250502 (2012).

[36] A. I. Lvovsky and J. Mlynek, Quantum-optical catalysis: Generating nonclassical states of light by means of linear optics, Phys. Rev. Lett. **88**, 250401 (2002).

[37] S. Scheel, K. Nemoto, W. J. Munro, and P. L. Knight, Measurement-induced nonlinearity in linear optics, Phys. Rev. A **68**, 032310 (2003).

[38] X.-X. Xu, Enhancing quantum entanglement and quantum teleportation for two-mode squeezed vacuum state by local quantum-optical catalysis, Phys. Rev. A **92**, 012318 (2015).

[39] S. Zhang and X. Zhang, Photon catalysis acting as noiseless linear amplification and its application in coherence enhancement, Phys. Rev. A **97**, 043830 (2018).

[40] Y. Guo, W. Ye, H. Zhong, and Q. Liao, Continuous-variable quantum key distribution with non-Gaussian quantum catalysis, Phys. Rev. A **99**, 032327 (2019).

[41] J.-S. Tang, Y.-L. Li, X.-Y. Xu, G.-Y. Xiang, C.-F. Li, and G.-C. Guo, Realization of quantum Wheeler's delayed-choice experiment, Nat. Photon. **6**, 600 (2012).

[42] C. M. Nunn, J. D. Franson, and T. B. Pittman, Heralding on the detection of zero photons, Phys. Rev. A **104**, 033717 (2021).

[43] D. R. M. Arvidsson-Shukur, N. Y. Halpern, H. V. Lepage, A. A. Lasek, C. H. W. Barnes, and S. Lloyd, Quantum advantage in postselected metrology, Nat. Commun. **11**, 3775 (2020).

[44] N. Lupu-Gladstein, Y. B. Yilmaz, D. R. M. Arvidsson-Shukur, A. Brodutch, A. O. T. Pang, A. M. Steinberg, and N. Y. Halpern, Negative quasiprobabilities enhance phase estimation in quantum-optics experiment, Phys. Rev. Lett. **128**, 220504 (2022).

[45] D. Gottesman and I. L. Chuang, Demonstrating the viability of universal quantum computation using teleportation and single-qubit operations, Nature (London) **402**, 390 (1999).

[46] D. Bouwmeester, J.-W. Pan, K. Mattle, M. Eibl, H. Weinfurter, and A. Zeilinger, Experimental quantum teleportation, Nature (London) **390**, 575 (1997).

[47] H. Ajiki, H. Ishihara, and K. Edamatsu, Cavity-assisted generation of entangled photons from a V-type three-level system, New J. Phys. **11**, 033033 (2009).

[48] D. H. Mahler, L. Rozema, K. Fisher, L. Vermeyden, K. J. Resch, H. M. Wiseman, and A. Steinberg, Experimental nonlocal and surreal Bohmian trajectories, Sci. Adv. **2**, e1501466 (2016).

[49] S. Das, S. Modak, and M. N. Bera, Saturating quantum advantages in postselected metrology with the positive Kirkwood-Dirac distribution, Phys. Rev. A **107**, 042413 (2023).

[50] P. A. M. Dirac, On the analogy between classical and quantum mechanics, Rev. Mod. Phys. **17**, 195 (1945).

[51] J. G. Kirkwood, Quantum statistics of almost classical assemblies, Phys. Rev. **44**, 31 (1933).

[52] L. M. Johansen, Quantum theory of successive projective measurements, Phys. Rev. A **76**, 012119 (2007).

[53] R. W. Spekkens, Negativity and contextuality are equivalent notions of nonclassicality, Phys. Rev. Lett. **101**, 020401 (2008).

[54] H. Margenau and R. N. Hill, Correlation between measurements in quantum theory, Prog. Theor. Phys. **26**, 722 (1961).

[55] S. Tanaka and N. Yamamoto, Information amplification via postselection: A parameter-estimation perspective, Phys. Rev. A **88**, 042116 (2013).

[56] J. Combes, C. Ferrie, Z. Jiang, and C. M. Caves, Quantum limits on postselected, probabilistic quantum metrology, Phys. Rev. A **89**, 052117 (2014).

[57] J. Fiurášek, Optimal linear-optical noiseless quantum amplifiers driven by auxiliary multiphoton Fock states, Phys. Rev. A **105**, 062425 (2022).